Aalborg Universitet

An Effective Model Predictive Control Method With Self-Balanced Capacitor Voltages for Single-Phase Three-Level Shunt Active Filters

Komurcugil, Hasan; Bayhan, Sertac; Guler, Naki; Blaabjerg, Frede

An Effective Model Predictive Control Method With Self-Balanced Capacitor Voltages for Single-Phase Three-Level Shunt Active Filters

HASAN KOMURCUGIL[1], **(Senior Member, IEEE), SERTAC BAYHAN**[2], **(Senior Member, IEEE), NAKI GULER**[3], **(Member, IEEE), AND FREDE BLAABJERG**[4], **(Fellow, IEEE)**

[1]Department of Computer Engineering, Eastern Mediterranean University, 99628 Famagusta, Turkey
[2]Qatar Environment and Energy Research Institute, Hamad Bin Khalifa University, Doha, Qatar
[3]Technical Sciences Vocational School, Gazi University, 06500 Ankara, Turkey
[4]The Faculty of Engineering and Science, Aalborg University, 9220 Aalborg, Denmark

Corresponding author: Sertac Bayhan (sbayhan@hbku.edu.qa)

ABSTRACT This paper presents an effective model predictive control (MPC) method for single-phase three-level T-type inverter-based shunt active power filters (SAPFs). The SAPF using T-type inverter topology has not been reported in the literature yet. Contrary to most of the existing MPC methods, the proposed MPC method eliminates the need for using weighting factor and additional constraints required for balancing dc capacitor voltages in the cost function. The design of cost function is based on the energy function. Since the factor used in the formulation of the energy function does not have any adverse influence on the performance of the system, the cost function becomes weighting factor free. The weighting factor free based MPC brings simplicity in the practical implementation. The effectiveness of the proposed MPC method has been investigated in steady-state as well as dynamic transients caused by load changes. The theoretical considerations are verified through experimental studies performed on a 3 kVA system.

INDEX TERMS Shunt active power filter, model predictive control, energy function.

I. INTRODUCTION

The widespread use of renewable energy sources, distributed generation sources, plug-in electric vehicles, and power-electronics loads such as consumer electronics, light emitting diode (LED) lights, electric drives, and diode rectifiers result in harmonic pollution in the power grid. Harmonic pollution deteriorates the power quality. Especially, the harmonic currents drawn by the aforementioned devices and loads increase losses, cause distortion in the grid voltage waveform, and cause interferences with the other devices connected at the point of common coupling (PCC). The power quality can be improved by using custom power devices such as static compensators [1], static VAR compensators [2], unified power quality controllers (UPQC) [3], dynamic voltage

restorers (DVR) [4], [5], and active power filters [6], [7]. Among these devices, the shunt active power filters (SAPF) offer effective solutions for load current related problems. The main function of an SAPF is to achieve sinusoidal grid currents at unity power factor by injecting the required current harmonics at PCC. However, the control of SAPF is challenging due to the fast-changing nature of the filter current. In order to obtain good performance, a fast current controller should be designed so that the actual filter current tracks the reference filter current with maximum tracking accuracy. This means that the designed current loop should have a high control bandwidth. On the other hand, the inverter topology used in the SAPFs also plays an important role in improving the power quality.

With the aim of achieving the desired control objectives, many control methods have been proposed in continuous-time [8]–[12]. Traditional proportional-integral (PI) control

The associate editor coordinating the review of this manuscript and approving it for publication was Ahmed A. Zaki Diab[ID].

method cannot offer satisfactory performance due to its limited control bandwidth [8]. Even though the linear quadratic regulator-based control method presented in [9] offers satisfactory performance, it involves too many control parameters, which should be tuned so as to obtain the desired performance. Lyapunov-function based control method offers fast response and assures global stability of the system at the expense of employing complicated controller in continuous-time [10]. Sliding mode control (SMC) approach exhibits fast current loop dynamics as well as simple implementation without parameter sensitivity [11]. However, it suffers from chattering, which leads to an uncontrollable switching frequency. Alternatively, the hysteresis current control method is also proposed which is robust to the parameter variations [12].

In the last decade, owing to the availability of powerful and cheap digital signal processors, numerous digital control techniques are proposed for SAPFs in discrete time. These digital control techniques include repetitive control [13]–[15], p-q theory-based control [16], deadbeat control [17], adaptive linear neural network based control [18], and predictive control [19]–[27]. The repetitive control method suppresses the periodic disturbances effectively, but its performance under non-periodic disturbances is not satisfactory. Even though the deadbeat control method has fast current loop dynamics, it is dependent on the system parameters, which cause performance degradation. In the last decade, the predictive control method has received considerable attention by many researchers due to its prominent advantages such as fast dynamic response and the prediction of future behavior of the controlled variables. The use of predicted variables results in obtaining the desired action determined by the preset optimization criterion. The first predictive control method applied to the control of SAPF was proposed in [19]. In [20], the properties of predictive control are combined with the artificial neural networks in generating the reference currents. The predictive control proposed in [21] is based on one-sample-period-ahead, which can predict the controlled variables one and two sampling periods in advance. Alternative to the classical predictive control method, model predictive control (MPC) has been introduced where a cost function is to be minimized [22], [23]. However, the use of weighting factor (WF) is essential in the cost function. The tuning of WF for a good performance is time consuming due to the lack of preset tuning procedure. Therefore, the tuning of WF is usually achieved by trial-and-error method. In addition, the tuned WF value is not unique and, therefore, it may not yield the same performance when the operating point of SAPF is changed. The finite control set MPC (FCS-MPC) method presented in [24] achieves suppression in the current ripple at the expense of using a modulator. Recently, a finite impulse response (FIR) based MPC is also introduced where the WF can be determined analytically [25]. In the aforementioned studies, the SAPF is based on two-level inverter topology.

In the last decade, the multilevel inverters (MIs) have received considerable attention by many researchers due

to the prominent advantages compared to the two-level inverters. For this reason, the MIs are widely employed in many applications including the SAPFs [26]–[28]. In [26], a three-phase three-level SAPF is realized by using cascaded H-bridge (CHB) inverters. The SAPF was controlled by using SMC technique, which suffers from chattering. Also, the control of dc-link voltage is difficult. In [27] and [28], the FCS-MPC method was applied to control a single-phase neutral-point clamped (NPC) inverter based SAPF and three-phase four-leg flying capacitor (FC) inverter based SAPF, respectively. The drawbacks of the NPC and FC inverter topologies are the clamping diode and flying capacitor requirements, which increase the cost and losses. On the other hand, both control methods do not need modulator. However, while the control method in [27] requires WF, the control method in [28] does not need WF at all. Among the MI topologies, the T-type inverter topology has fewer components with same number of levels [29]. However, the MPC method has not been analyzed yet in the case of three-level T-type inverter operating as SAPF.

In this paper, an effective MPC method is proposed for a single-phase three-level T-type inverter based SAPF. Unlike the existing MPC methods, the proposed control method does not employ WF in the cost function. In addition, the capacitor voltages are balanced without using an additional constraint in the cost function as mentioned in [30]. Therefore, a simplification is obtained in the design phase. The optimum switching states, which force the error variables to zero, are determined from the derivative of the energy function. The negative definiteness of the energy function assures the stability of the system. Extensive experimental results are presented to validate the proposed control approach.
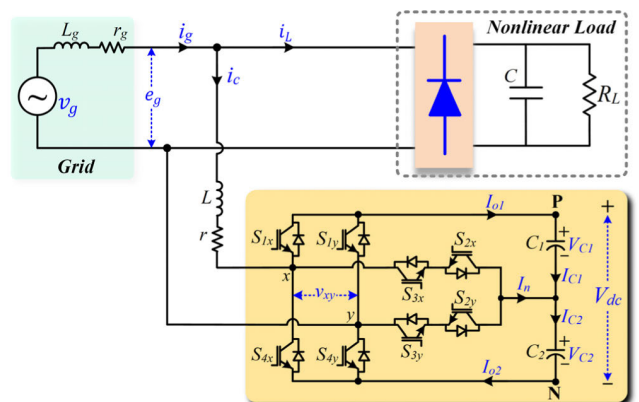

FIGURE 1. Single-phase three-level T-type inverter-based SAPF.

II. MODELING OF SAPF
The single-phase three-level SAPF using a T-type inverter is depicted in Fig. 1. Clearly, the SAPF has four switches per each leg. The state of each switch is defined as

$$S_{ij} = \begin{cases} 1 & \text{closed} \\ 0 & \text{open} \end{cases} \tag{1}$$

TABLE 1. Operating states, switching states and pole voltages.

Operating State	S_{1j}	S_{2j}	S_{3j}	S_{4j}	v_{jo}
P	ON	ON	OFF	OFF	$+V_{dc}/2$
O	OFF	ON	ON	OFF	0
N	OFF	OFF	ON	ON	$-V_{dc}/2$

where $i = 1, 2, 3, 4$ and $j = x, y$. The SAPF produces three different pole voltages with respect to the neutral point O. These voltages exist when the midpoint of each rectifier leg is connected to positive (P), neutral (O) and negative (N) points via proper switching. The operating states, states of switching devices and produced pole voltages are shown in Table 1. Apparently, the SAPF operates in the P state producing a pole voltage $v_{jO} = +V_{dc}/2$ when S_{1j} and S_{2j} are closed (ON) and S_{3j} and S_{4j} are open (OFF). On the other hand, the rectifier operates in the O state which produces a pole voltage $v_{jO} = 0$ V when S_{2j} and S_{3j} are ON and S_{1j} and S_{4j} are OFF. Finally, the SAPF operates in the N state producing pole voltage $v_{jO} = -V_{dc}/2$ when S_{1j} and S_{2j} are OFF and S_{3j} and S_{4j} are ON.

The control input switching functions of the rectifier can be defined as

$$S_1 = S_{1x} - S_{1y} \qquad (2)$$
$$S_2 = S_{2x} - S_{2y} \qquad (3)$$

The three-level input voltage and neutral current can be defined in terms of the switching functions as follows

$$v_{xy} = S_1 V_{C1} + S_2 V_{C2} \qquad (4)$$
$$I_n = I_{C2} - I_{C1} = (S_2 - S_1)i_c \qquad (5)$$

By making use of different switching combinations, v_{xy} can be generated as a five-level voltage with levels 0, $\pm V_{dc}/2$, and $\pm V_{dc}$.

The differential equations of the SAPF can be written as

$$\frac{di_c}{dt} = \frac{1}{L}(e_g - v_{xy} - ri_c) \qquad (6)$$
$$\frac{dV_{dc}}{dt} = \frac{2I_{o1}}{C_1} \qquad (7)$$

where $v_{xy} = uV_{dc}$, $I_{o1} = ui_c$, u is the switching function. In the derivation of (7), it is assumed that $V_{C1} = V_{dc}/2$. On the other hand, the capacitor currents in terms of the switching functions (S_1 and S_2) and grid current are obtained as

$$I_{C1} = \frac{1}{2}(S_1 i_c - S_2 i_c) \qquad (8)$$
$$I_{C2} = \frac{1}{2}(S_2 i_c - S_1 i_c) \qquad (9)$$

The design of the passive components (filter inductance and dc capacitors) are calculated as follows [31], [32]

$$L_{max} = \frac{v_g}{2\sqrt{2}f_s \Delta i_c} \qquad (10)$$
$$C_1 = C_2 = \frac{v_g I_{c\,max}}{2f\left[V_{dc}^2 - V_{dc\,min}^2\right]} \qquad (11)$$

where L_{max} is the maximum value of filter inductance, i_c is the high frequency ripple in compensation current (i_c), f_s is switching frequency, $I_{C\max}$ is the maximum compensation current, f is the grid frequency and $V_{dc\,min}$ is the minimum dc side voltage. Using parameters listed in Table 2 (see Section IV), the maximum filter inductance is calculated as 2.62mH for 9kHz average switching frequency and 15% ripple ratio in i_c. It is worth noting that the filter inductance (L) used in the experimental setup was selected to be 2mH. It should be noted that the minimum V_{dc} should be larger than the peak value of grid voltage. Since the experimental tests are performed using 120V rms grid voltage, $V_{dc\,min}$ is selected to be 170V. Substituting $v_g = 120$V, $I_{C\max} = 12$A, $f = 50$Hz, $V_{dc} = 250$V and $V_{dc\,min} = 170$V into (11), we obtain the values of C_1 and C_2 as 428μF. Since these values are not available, 470μF capacitors are used in the experimental setup.

III. ENERGY FUNCTION BASED MPC

The block diagram of the developed energy function based MPC technique is depicted in Fig. 2. The proposed approach consists of the following two steps.
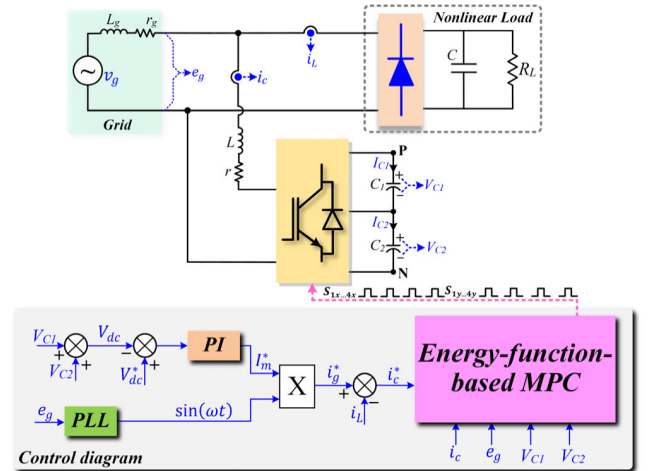
FIGURE 2. Block diagram of the proposed energy function-based MPC with three-level T-type inverter based SAPF.

A. DESIGN OF ENERGY FUNCTION BASED MPC

The main control objectives of the three-level SAPF are to regulate V_{dc} to its reference, regulate capacitor voltages, obtain sinusoidal grid current at unity power factor, and guarantee stable operation under various load types. It is worth to note that when the regulation of V_{dc} is accomplished, the control of capacitor voltages is achieved automatically. Also, the unity power factor operation occurs when the grid current is in phase with the grid voltage. In order to meet the latter objective, the grid voltage and reference grid current should be in the form of

$$e_g = E_m \sin(\omega t), \quad i_g^* = I_m^* \sin(\omega t) \qquad (12)$$

The sine wave template in i_g^* is obtained via a classical phase locked loop (PLL). The amplitude of reference grid current is produced by a proportional-integral (PI) regulator as follows

$$I_m^* = K_p(V_{dc}^* - V_{dc}) + K_i \int (V_{dc}^* - V_{dc})dt \qquad (13)$$

where K_p and K_i are proportional and integral gains, respectively and V_{dc}^* is reference of V_{dc}. From (6), it follows that the derivative of i_c^* can be written as

$$\frac{di_c^*}{dt} = \frac{1}{L}(e_g - v_{xy}^* - ri_c^*) \qquad (14)$$

where i_c^* denotes the reference of i_c, which is defined as

$$i_c^* = i_g^* - i_L \qquad (15)$$

In (15), the measurement of i_L is required. Unlike the classical MPC involving a cost function, the proposed MPC employs an energy function. It can be seen from Fig. 2 that there are two dc-side capacitors and one ac-side inductor, which have the ability to store energy in the SAPF. Therefore, the energy function in the continuous-time can be expressed in terms of capacitor voltage error (x_1) and inductor current error (x_2) as follows

$$E(x) = \frac{1}{2}\beta_1 x_1^2 + \frac{1}{2}\beta_2 x_2^2 \qquad (16)$$

where the constants β_1 and β_2 should be positive and x_1 and x_2 are the error variables defined as follows

$$x_1 = V_{C1} - V_{C2}, \quad x_2 = i_c - i_c^* \qquad (17)$$

It can be noticed that equation (16) is in the form of energy stored in inductor and capacitor. For instance, the first term in (16) gives the energy stored in capacitor while the second term is the energy stored in inductor. The details of formulating $E(x)$ can be found in [33] and [34]. It is worth noting that inclusion of x_1 in $E(x)$ has a self-balanced effect on the dc capacitor voltages. Now, taking the derivative of (17) and making use of (6), (8), (9), and (14) yields

$$\dot{x}_1 = \frac{1}{2C_1}(S_1 i_c - S_2 i_c) - \frac{1}{2C_2}(S_2 i_c - S_1 i_c) \qquad (18)$$

$$\dot{x}_2 = \frac{1}{L}(v_{xy}^* - v_{xy} - rx_2) \qquad (19)$$

Equations (18) and (19) denote the dynamics of error variables in (17).

The energy function should satisfy the following conditions

  i) $E(x) > 0$ when $x_1 \neq 0$ and $x_2 \neq 0$
  ii) $E(x) \to \infty$ when $\|x_1\| \to \infty$ and $\|x_2\| \to \infty$
  iii) $\dot{E}(x) < 0$

Clearly, the first two conditions are satisfied. The third condition (negative definiteness of $E(x)$) which guarantees the stability of the system should also be satisfied. It is worth to note that $E(x)$ increases or decreases depending on the values of x_1 and x_2. When the error variables converge to zero ($x_1 = 0$ and $x_2 = 0$), $E(x)$ also tends to zero. Therefore, the main goal is to minimize $E(x)$ and at the same time achieve $\dot{E}(x) < 0$.

Taking the derivative of (16) yields

$$\dot{E}(x) = \beta_1 \dot{x}_1 x_1 + \beta_2 \dot{x}_2 x_2 \qquad (20)$$

Now, substituting (4), (18) and (19) into (20) gives

$$\dot{E}(x) = \frac{\beta_1}{2C_1}(S_1 i_c - S_2 i_c)x_1 - \frac{\beta_1}{2C_2}(S_2 i_c - S_1 i_c)x_1$$
$$+ \frac{\beta_2}{L}(v_{xy}^* - S_1 V_{C1} - S_2 V_{C2} - rx_2)x_2 \qquad (21)$$

Substituting $i_c = x_2 + i_c^*$ into (21) and assuming that $C_1 = C_2 = C$, one can obtain

$$\dot{E}(x) = S_1 x_1 x_2 \left(\frac{\beta_1}{C} - \frac{\beta_2}{L}\right) + S_2 x_1 x_2 \left(\frac{\beta_2}{L} - \frac{\beta_1}{C}\right)$$
$$+ \frac{\beta_1}{C}(S_1 - S_2) i_c^* x_1$$
$$+ \frac{\beta_2}{L}\left(v_{xy}^* x_2 - S_1 V_{C1} x_2 - S_2 V_{C2} x_2 - rx_2^2\right) \qquad (22)$$

Selecting $\beta_1 = C\beta_2/L$ eliminates the terms $S_1 x_1 x_2$ and $S_2 x_1 x_2$ which also reduces equation (22) to

$$\dot{E}(x) = \frac{\beta_2}{L}\left((S_1 - S_2)i_c^* x_1 + v_{xy}^* x_2 - S_1 V_{C1} x_2 \right.$$
$$\left. - S_2 V_{C2} x_2 - rx_2^2\right) \qquad (23)$$

The stability of the closed-loop system is assured if $\dot{E}(x) < 0$. The main aim in this study is to design MPC strategy by using (23). Since equation (23) is in continuous time, it should be expressed in discrete time to design the MPC.

B. DISCRETE-TIME MODEL

Now, $\dot{E}(x)$ in (23) can be expressed in discrete time at $(k+1)^{th}$ sampling instant as follows

$$\dot{E}_x^{(n)}(k+1)$$
$$= \frac{\beta_2}{L}((S_1^{(n)}(k) - S_2^{(n)}(k))i_c^*(k+1)x_1(k+1)$$
$$+ v_{xy}^*(k+1)x_2(k+1) - S_1^{(n)}(k)V_{C1}(k+1)x_2(k+1)$$
$$- S_2^{(n)}(k)V_{C2}(k+1)x_2(k+1) - rx_2^2(k+1)) \qquad (24)$$

Equation (24) can be used to select the optimum switching functions $S_1(k)$ and $S_2(k)$ such that $\dot{E}_x(k+1)$ is negative. It is worth to note that the choice of β_2/L has no effect on the performance of the controller provided that $\beta_2 > 0$. In order to verify this claim, the performance of the proposed energy function based MPC is investigated by using various β_2 values (see Fig. 11(b)). It can be observed that once $\dot{E}_x(k+1) < 0$ is achieved, the system works successfully regardless of β_2 values. Therefore, unlike the classical MPC method whose performance depends on WF, the proposed MPC method is WF free that yields a simplification in the design of the controller. The error variables in (24) can be written as

$$x_1(k+1) = V_{C1}(k+1) - V_{C2}(k+1) \qquad (25)$$
$$x_2(k+1) = i_c(k+1) - i_c^*(k+1) \qquad (26)$$

Algorithm 1 Energy Function Based MPC

1: Measure $e_g(k)$, $i_c(k)$, $V_{C1}(k)$, and $V_{C2}(k)$.
2: Compute $i_c(k)$.
3: Compute (31)-(33).
4:     **for** $n = 1,\ldots.., 9$ **do**
5:       Compute (25) and (26).
6:       Evaluate (24).
7:     **end for**
8: **return** minimum $\dot{E}_x(k+1)$.
9: Choose switching states which yield minimum $\dot{E}_x(k+1)$.

Applying the first order forward Euler approximation to (6), (8), and (9), the future values of $i_c(k)$, $V_{C1}(k)$, and $V_{C2}(k)$ at $(k+1)^{th}$ sampling instant can be obtained as follows

$$i_c(k+1) = (1 - \frac{r}{L}T_s)i_c(k) + \frac{T_s}{L}\left(e_g(k) - v_{xy}(k)\right) \quad (27)$$

$$V_{C1}(k+1) = V_{C1}(k) + \frac{T_s}{2C_1}\left(S_1(k)i_c(k) - S_2(k)i_c(k)\right) \quad (28)$$

$$V_{C2}(k+1) = V_{C2}(k) + \frac{T_s}{2C_2}\left(S_2(k)i_c(k) + S_1(k)i_c(k)\right) \quad (29)$$

where T_s is the sampling period and $v_{xy}(k)$ is given by

$$v_{xy}(k) = S_1(k)V_{C1}(k) + S_2(k)V_{C2}(k) \quad (30)$$

On the other hand, the grid voltage, reference grid current and input voltage of rectifier at $(k+1)^{th}$ sampling instant which are needed in (24) can be predicted as

$$e_g(k+1) = \frac{3}{2}e_g(k) - \frac{1}{2}e_g(k-1) \quad (31)$$

$$i_c^*(k+1) = \frac{3}{2}i_c^*(k) - \frac{1}{2}i_c^*(k-1) \quad (32)$$

$$v_{xy}^*(k+1) = e_g(k+1) - \frac{L}{T_s}\left(i_c^*(k+1) - i_c^*(k)\right)$$
$$- ri_c^*(k+1) \quad (33)$$

The steps of the proposed energy function based MPC method are given in the Algorithm. First, the system variables are measured to be used in the control algorithm. Then, the compensation current reference (i_c^*) is computed. The predictions of $e_g(k+1)$, $i_c^*(k+1)$ and $v_{xy}^*(k+1)$ are calculated to be used in the energy function. Thereafter, the predicted values of the error variables ($x_1(k+1)$ and $x_2(k+1)$) are calculated for each possible switching state. The derivative of energy function ($\dot{E}_x(k+1)$) is evaluated using the predicted values in the previous steps. In the last step, the optimal switching vector is determined by minimizing $\dot{E}_x(k+1)$. The flowchart of the proposed MPC algorithm is given in Fig. 3.

IV. EXPERIMENTAL VERIFICATION

The effectiveness of the proposed MPC method is verified by experimental studies by implementing the block diagram shown in Fig. 2. In the experimental studies, a full-wave diode-bridge rectifier is used as the nonlinear load. The experimental studies have been carried out on the prototype shown in Fig. 4 where the power grid is emulated via a regenerative
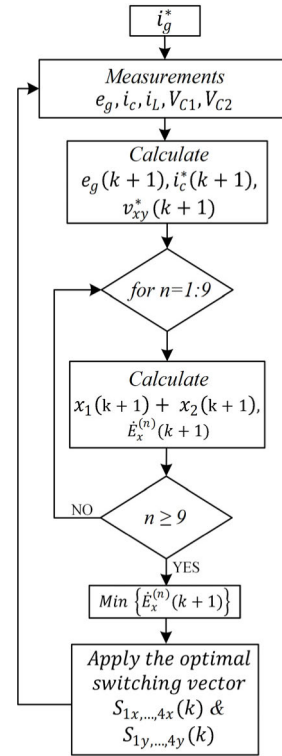
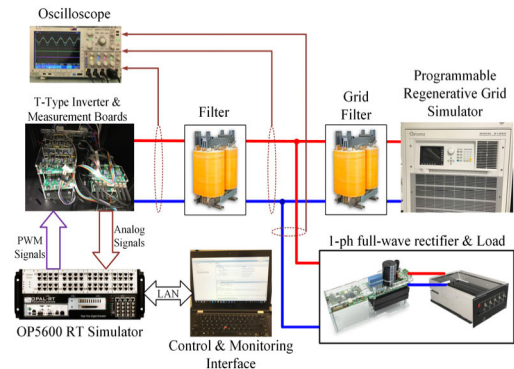**FIGURE 3.** Flowchart of the proposed energy-function-based FCS-MPC.

FIGURE 4. Experimental setup for the SAPF.

grid simulator (Chroma 61860). The proposed MPC method was implemented by using OPAL-RT OP5600. The pulse width modulation (PWM) signals generated by OPAL-RT are applied to drive the switches in the T-type inverter. The system and control parameters used in the experimental studies are listed in Table 2.

A. STEADY-STATE AND DYNAMIC RESPONSE TESTS

Fig. 5 shows the waveforms of grid voltage (e_g), grid current (i_g), load current (i_L), filter current (i_c), filter current reference (i_c^*), dc-link voltage (V_{dc}), dc-link voltage reference (V_{dc}^*) and capacitor voltages (V_{C1}, V_{C2}). Despite the highly distorted load current, the grid current is sinusoidal and in

TABLE 2. System and control parameters.

Description and Symbol	Value
Grid voltage amplitude: E_m	$120\sqrt{2}$ V
DC-link voltage reference: V_{dc}^*	250 V
Inductance: L	2 mH
Inductor resistance: r	0.1 Ω
Grid inductance: L_g	2 mH
Inductor resistance: r_g	0.1 Ω
DC capacitors: $C_1 = C_2$	470 μF
Nonlinear load (R_L , C)	25 Ω, 470 μF
PI gains: K_p , K_i	0.3, 5
Controller gain: β_2	1
Sampling time: T_s	50 μs

phase with the grid voltage. Hence, the unity power factor operation is achieved. The filter current and its reference are overlapped, which implies that the controller has almost zero tracking error. It is obvious that the control of the dc-link and capacitor voltages is achieved at 250V and 125V, respectively.
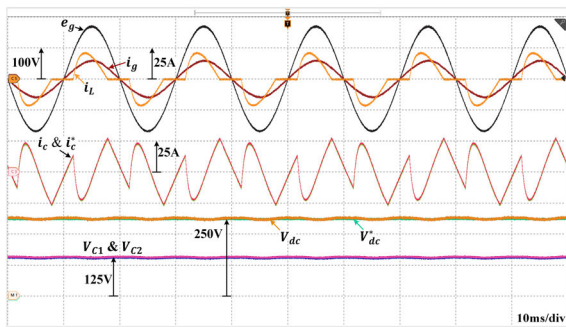

FIGURE 5. Waveforms of grid-voltage (e_g), grid current (i_g), load current (i_L), filter current (i_c), filter current reference (i_c^*), dc-link voltage (V_{dc}), dc-link voltage reference (V_{dc}^*), and capacitor voltages (V_{C1} and V_{C2}).
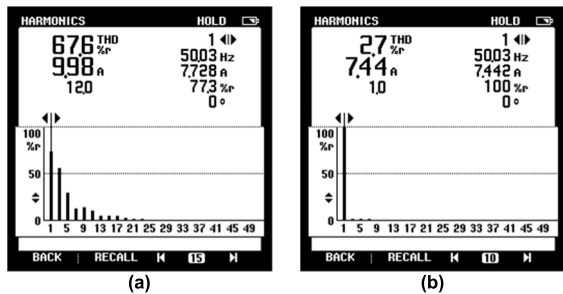

FIGURE 6. Measured spectrums of load and grid currents corresponding to Fig. 5. (a) Load current spectrum, (b) Grid current spectrum.

Fig. 6 shows the spectrums of load and grid currents corresponding to Fig. 5. It can be seen from Fig. 6(a) that the load current contains significant odd harmonic components. The measured THD of load current is 67.6%. On the other hand, the majority of odd harmonic components in the grid current
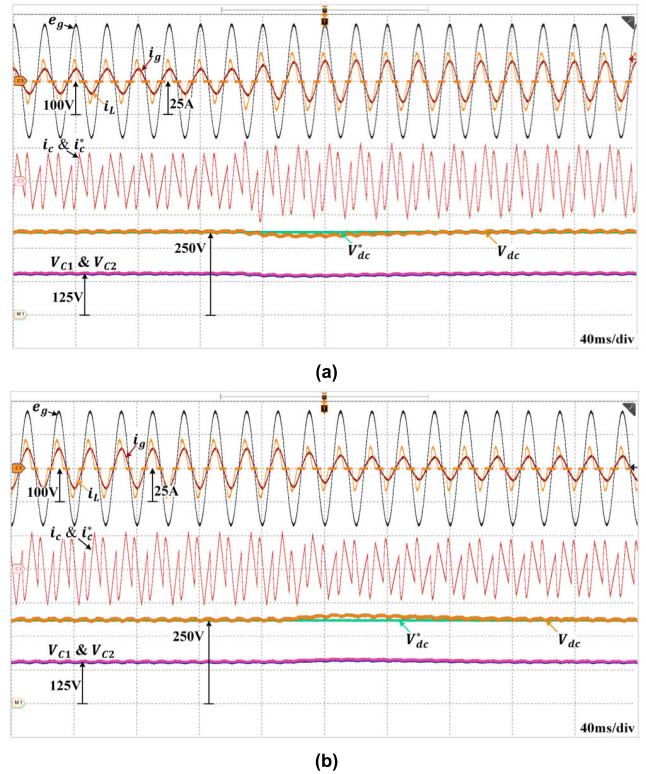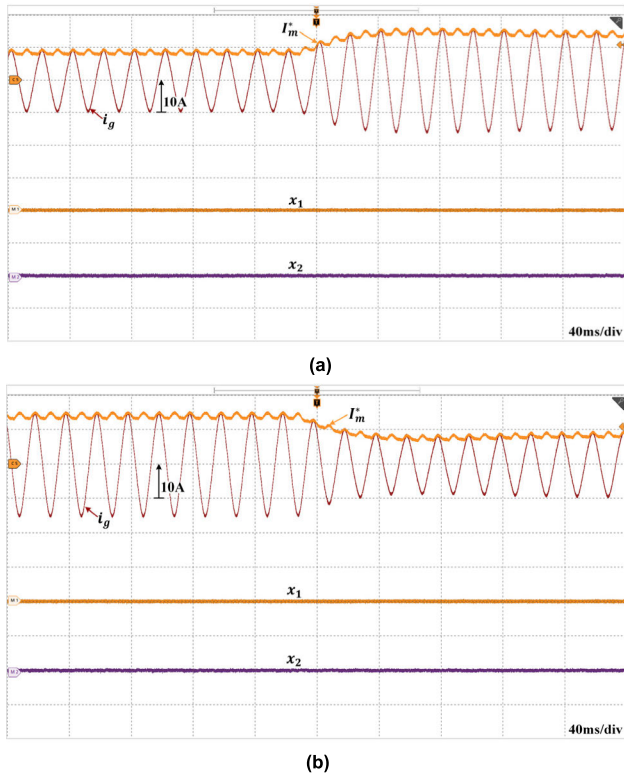

FIGURE 7. Waveforms of grid-voltage (e_g), grid current (i_g), load current (i_L), filter current (i_c), filter current reference (i_c^*), dc-link voltage (V_{dc}), dc-link voltage reference (V_{dc}^*), and capacitor voltages (V_{C1} and V_{C2}) for step change in load current. (a) Load current is increased, (b) Load current is decreased.

are suppressed as shown in Fig. 6(b). Clearly, only the 3rd, 5th, and 7th harmonic components are discernible with small magnitudes. Majority of odd harmonic components such as 9th, 11th, 13th, 15th, and other components are suppressed effectively. As a consequence of this fact, the THD of grid current is measured to be 2.7%. The effectiveness of the proposed controller on the operation of SAPF can be understood if the measured THD values are considered. Comparing the measured THD values of load and grid currents, one can see that the proposed SAPF operates with high performance.

Fig. 7 shows operation of the SAPF for a step change in the nonlinear load current. It is worth noting that all variables are regulated before the step change occurs. When the load current increases (dc load resistance has been changed from 25 Ω to 12.5 Ω), the dc-link voltage exhibits small undershoot and tracks its reference successfully as shown in Fig. 7(a). The capacitor voltages behave similar to the dc-link voltage. The grid current is also increased in response to the load current increment. On the other hand, when the load current is decreased (dc load resistance has been changed from 12.5 Ω to 25 Ω), the dc-link voltage gives rise to small overshoot and tracks its reference successfully after the transient is over as shown in Fig. 7(b). Similarly, the capacitor voltages are also regulated in this case. Finally, it can be seen that the grid current is decreased in response to the decrement in load current.

(a)

(b)

FIGURE 8. Waveforms of grid current (i_g), PI output (I_m^*), capacitor voltage error (x_1) and filter current error (x_2) corresponding to the load current changes in Fig. 7. (a) Load current is increased, (b) Load current is decreased.

Fig. 8 shows the waveforms of grid current, PI output, capacitor voltage error and filter current error corresponding to the load current changes in Fig. 8. Apparently, the grid current increases so as to track its reference when the load current is increased as shown in Fig. 8(a). Similarly, as a result of decrement in the load current, the grid current decreases as well and tracks its reference as shown in Fig. 8(b). In both cases, the error variables are completely zero, which indicate that the proposed controller acts very fast in tracking the references.

Fig. 9 shows the waveforms of grid voltage, grid current, load current (i_L), filter current, dc-link voltage and capacitor voltages for start-up. Initially, the system is started with SAPF disabled. In this case, the grid current is equal to the load current and, eventually, the filter current is zero. The dc-link and capacitor voltages are also zero. When the SAPF is enabled, the filter current is not zero anymore, which implies that the grid current and load current are not equal. In this case, the filter current is added with the load current at the point of common coupling such that the grid current becomes sinusoidal and in phase with grid voltage. On the other hand, dc-link and capacitor voltages gradually converge to 250V and 125V, respectively.

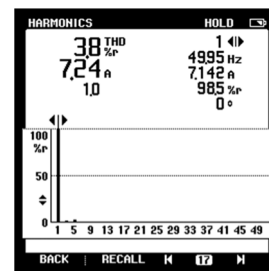### B. COMPARISON WITH CLASSICAL MPC METHOD
Fig. 10 shows operation of SAPF under classical MPC that employs a WF. Even though the control of dc-link and
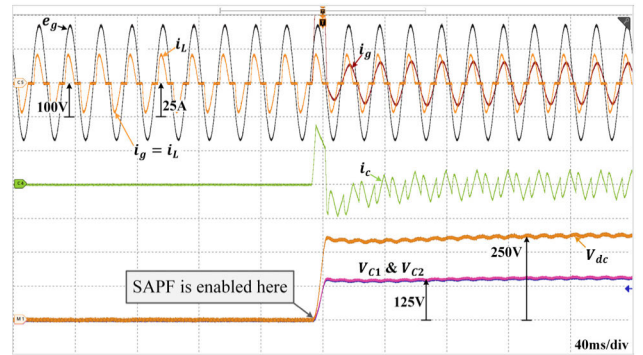
FIGURE 9. Waveforms of grid-voltage (e_g), grid current (i_g), load current (i_L), filter current (i_c), dc-link voltage (V_{dc}), and capacitor voltages (V_{C1} and V_{C2}) for start-up.
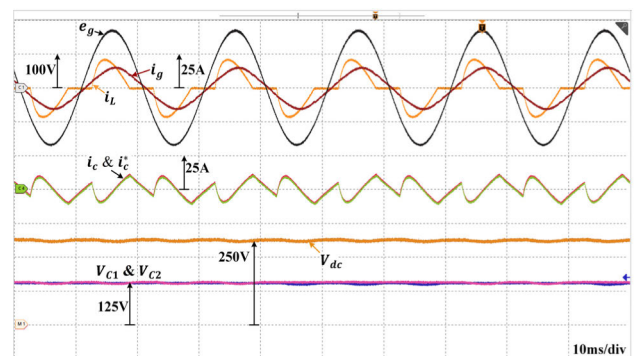
(a)

(b)

FIGURE 10. Operation of SAPF under classical MPC; (a) Waveforms of grid-voltage (e_g), grid current (i_g), load current (i_L), filter current (i_c), filter current reference (i_c^*), dc-link voltage (V_{dc}), and capacitor voltages (V_{C1} and V_{C2}), (b) Spectrum of grid current (i_g).

capacitor voltages is accomplished and the grid current is sinusoidal, the unity power factor is not satisfied completely as shown in Fig. 10(a). The spectrum of grid current is presented in Fig. 10(b). The THD of grid current is measured as 3.80%. Comparing the THDs of grid current obtained by proposed MPC and classical MPC, one can see that the proposed MPC method yields smaller THD value as shown in Fig. 6(b).

Fig. 11 shows the waveforms obtained by the classical and proposed MPC methods for a step variation in WF and β_2, respectively. It is worth noting that the control of dc-link and capacitor voltages and reactive power compensation together with the unity power factor are satisfied before the step change in WF as shown in Fig. 11(a). However, when the WF

(a)

(b)

FIGURE 11. Waveforms of grid-voltage (e_g), grid current (i_g), load current (i_L), filter current (i_c), dc-link voltage ($V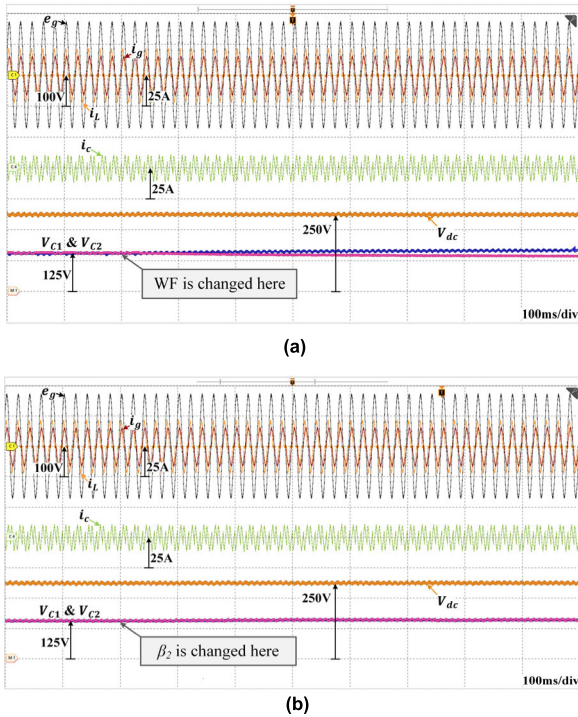_{dc}$), and capacitor voltages (V_{C1} and V_{C2}) obtained by: (a) Classical MPC for a step change in WF from 1 to 10, (b) Proposed MPC for a step change in β_2 from 1 to 10.

value is changed from 1 to 10, the capacitor voltages deviate from 125 V and become unbalanced. If the system is operated with WF = 10 for a long time, it would adversely affect the operation of SAPF since the control of dc-link voltage will be lost. This can be considered as the main disadvantage of the classical MPC that is dependent on the WF value. In literature, no procedure for tuning the WF for optimum performance is reported. The tuning of WF is usually achieved by trial-and-error method. On the other hand, changing β_2 value from 1 to 10 has no effect on the operation of the system as shown in Fig. 11(b). Since the proposed MPC does not require the WF, it brings a simplification in the design of the controller.
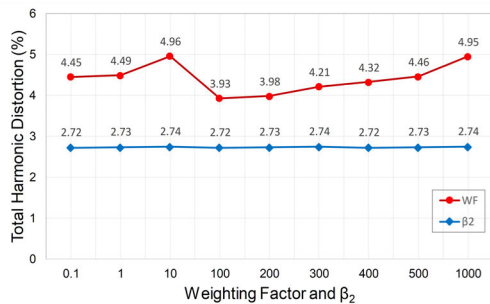
FIGURE 12. THD comparison of classical and proposed MPC methods under weighting factor and β_2 variations.

Fig. 12 shows the influence of varying WF and β_2 on the THD of grid current. It is evident that the THD is subject to
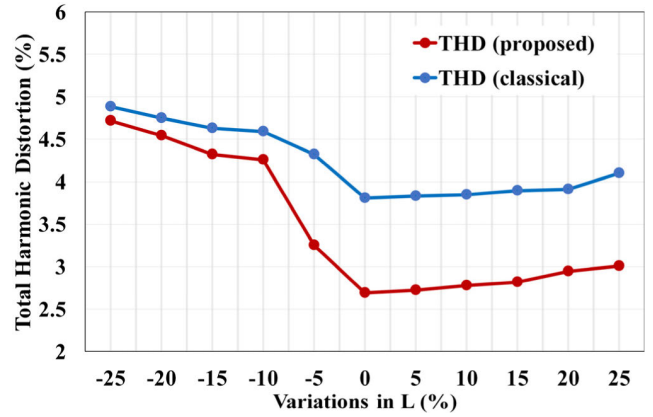
FIGURE 13. Experimental results of the robustness analysis with parameter variations in filter inductance (L).

the WF value variations. This result clearly shows the disadvantage of classical MPC in which WF tuning is essential to obtain good performance. Since there is no preset rule for tuning WF, the design of WF becomes challenging in some applications. However, the THD is not affected when the value of β_2 is increased. Contrary to the classical MPC, the coefficient (β_2) employed in the cost function of the proposed MPC has no effect on the THD of grid current.

The proposed energy function based MPC method is also compared with five control methods presented in [27] and [35]–[38]. The comparison is based on the type of controller, weighting factor necessity, number of weighting factors, number of required sensors, additional controller necessity for controlling dc capacitor voltages, and reference filter current generation method as shown in Table 3.

Obviously, the proposed energy based MPC method is beneficial in terms of weighting factor free structure, reduced controller complexity as it does not need additional control loop for dc capacitor voltage regulation and reference filter current generation. The proposed energy function based MPC method possesses weighting factor free structure, which offers simplicity in the design. Opposed to [27] and [35]–[37], the proposed method in this study and [38] does not need an additional controller for regulating dc capacitor voltages. However, the control method in [38] needs weighting factor and requires one extra sensor compared to the proposed method here. On the other hand, contrary to the filter current reference generation in the proposed method, the methods in [27] and [35]–[37] require many computations, additional transformations, low pass filter and high pass filter.

C. ROBUSTNESS ANALYSIS

Since the proposed control method is dependent on the system parameters, the robustness of the control approach to parameter variations is essential. For comparison purposes, the robustness of the classical MPC method is also investigated. The results that are obtained under the same operating conditions in Fig. 5 and Fig. 10(a) are presented in Fig. 13.

TABLE 3. Comparison of five control methods with proposed energy function based MPC method.

Description	[27]	[35]	[36]	[37]	[38]	Proposed
Topology	1ϕ NPC-SAPF	1ϕ CHB-SAPF	1ϕ 5 Level-SAPF	1ϕ CHB-SAPF	1ϕ MPUC5 - SAPF	1ϕ T-type-SAPF
Controller	FCS-MPC	model-based controller	Predictive current controller	Direct current control	FCS-MPC	Energy-MPC
Weighting factor	Not needed	N/A	Not needed	N/A	Needed	Not needed
Number of weighting factors	N/A	N/A	N/A	N/A	1	N/A
Number of sensors	6	5	5	5	6	5
Components required in the topology	2 DC capacitors, 1 inductor, 8 switches and 4 diodes	2 DC capacitors, 1 inductor and 8 switches	2 DC capacitors, 2 diodes, 1 inductor and 6 switches	2 DC capacitors, 1 inductor and 8 switches	2 DC capacitors, 1 inductor and 6 switches	2 DC capacitors, 1 inductor and 8 switches
Additional controller requirement for dc capacitor voltages	Needed	Needed	Needed	Needed	Not needed	Not needed
Reference filter current generation method	5 multiplications, 2 additions, and 2 low pass filters are needed	RMS calculation, current tracking loop and harmonic oscillators are needed	Transformation to αβ frame, p-q theory and predictive current controller are needed	Transformation to dq frame, 3 transformations to ab frame, 1 high pass filter and 3 PI controllers are needed	1 subtraction is needed	1 subtraction is needed ($i_c^* = i_g^* - i_L$)

ϕ: Phase, N/A: Not applicable

The inductance parameter (L) in the control software was varied from -25% to 25% by gradual increments in L. As clearly seen in Fig. 13, the lowest THD values are obtained by both control methods when L in the control software is equal to the actual L in the experimental setup. Clearly, the THD values of both methods are increased when the mismatch in L increases. The maximum THD value is measured when the mismatch in L is −25%. However, the THD value obtained by the proposed control method is always smaller than the classical MPC method for the same mismatch range.

V. CONCLUSION

An energy function based MPC method is proposed for single-phase three-level T-type inverter based SAPFs. Unlike the existing MPC methods, the proposed MPC method eliminates the need for using weighting factor in the cost function. The design of the cost function in the proposed MPC is based on the negative definiteness of the rate of change of energy function. Furthermore, the proposed MPC method is able to stabilize the dc capacitor voltages without using additional constraints in the cost function. Among the MPC methods developed for multilevel SAPFs, the proposed MPC has the simplest structure. The performance of the proposed MPC method has been verified under steady-state and transients caused by the load variations. Also, the performances of the proposed and classical MPC methods are compared in terms of grid current THD and influence of WF variations. It is pointed out that the performance of the proposed MPC and grid current THD are not affected from the variations in WF value.

REFERENCES

[1] S. W. Mohod and M. V. Aware, "A STATCOM-control scheme for grid connected wind energy system for power quality improvement," *IEEE Syst. J.*, vol. 4, no. 3, pp. 346–352, Sep. 2010.

[2] A. Hamadi, S. Rahmani, and K. Al-Haddad, "A hybrid passive filter configuration for VAR control and harmonic compensation," *IEEE Trans. Ind. Electron.*, vol. 57, no. 7, pp. 2419–2434, Jul. 2010.

[3] V. Khadkikar, "Enhancing electric power quality using UPQC: A comprehensive overview," *IEEE Trans. Power Electron.*, vol. 27, no. 5, pp. 2284–2297, May 2012.

[4] H. Komurcugil and S. Biricik, "Time-varying and constant switching frequency-based sliding-mode control methods for transformerless DVR employing half-bridge VSI," *IEEE Trans. Ind. Electron.*, vol. 64, no. 4, pp. 2570–2579, Apr. 2017.

[5] S. Biricik, H. Komurcugil, N. D. Tuyen, and A. Basu, "Protection of sensitive loads using sliding mode controlled three-phase DVR with adaptive notch filter," *IEEE Trans. Ind. Electron.*, vol. 66, no. 7, pp. 5465–5475, Jul. 2019.

[6] B. Singh, K. Al-Haddad, and A. Chandra, "A review of active filters for power quality improvement," *IEEE Trans. Ind. Electron.*, vol. 46, no. 5, pp. 960–971, Oct. 1999.

[7] M. El-Habrouk, M. K. Darwish, and P. Mehta, "Active power filters: A review," *IEE Elect. Power Appl.*, vol. 147, no. 5, pp. 403–413, Sep. 2000.

[8] S. Rahmani, N. Mendalek, and K. Al-Haddad, "Experimental design of a nonlinear control technique for three-phase shunt active power filter," *IEEE Trans. Ind. Electron.*, vol. 57, no. 10, pp. 3364–3375, Oct. 2010.

[9] B. Kedjar and K. Al-Haddad, "DSP-based implementation of an LQR with integral action for a three-phase three-wire shunt active power filter," *IEEE Trans. Ind. Electron.*, vol. 56, no. 8, pp. 2821–2828, Aug. 2009.

[10] H. Komurcugil and O. Kukrer, "A new control strategy for single-phase shunt active power filters using a Lyapunov function," *IEEE Trans. Ind. Electron.*, vol. 53, no. 1, pp. 305–312, Feb. 2006.

[11] J. Fei and H. Wang, "Experimental investigation of recurrent neural network fractional-order sliding mode control of active power filter," *IEEE Trans. Circuits Syst. II, Exp. Briefs*, vol. 67, no. 11, pp. 2522–2526, Nov. 2019.

[12] H. Komurcugil, "Double-band hysteresis current-controlled single-phase shunt active power filter for switching frequency mitigation," *Int. J. Electr. Power Energy Syst.*, vol. 69, pp. 131–140, Jul. 2015.

[13] Z. X. Zou, K. Zhou, Z. Wang, and M. Cheng, "Frequency-adaptive fractional-order repetitive control of shunt active power filters," *IEEE Trans. Ind. Electron.*, vol. 62, no. 3, pp. 1659–1668, Mar. 2015.

[14] C. Xie, X. Zhao, M. Savaghebi, L. Meng, J. M. Guerrero, and J. C. Vasquez, "Multirate fractional-order repetitive control of shunt active power filter suitable for microgrid applications," *IEEE J. Emerg. Sel. Topics Power Electronics*, vol. 5, no. 2, pp. 809–819, Jun. 2017.

[15] G. Pandove and M. Singh, "Robust repetitive control design for a three-phase four wire shunt active power filter," *IEEE Trans. Ind. Informat.*, vol. 15, no. 5, pp. 2810–2818, May 2019.

[16] M. Popescu, A. Bitoleanu, and V. Suru, "A DSP-based implementation of the p-q theory in active power filtering under nonideal voltage conditions," *IEEE Trans. Ind. Informat.*, vol. 9, no. 2, pp. 880–889, May 2013.

[17] V. Biagini, P. Zanchetta, M. Odavic, M. Sumner, and M. Degano, "Control and modulation of a multilevel active filtering solution for variable-speed constant-frequency more-electric aircraft grids," *IEEE Trans. Ind. Informat.*, vol. 9, no. 2, pp. 600–608, May 2013.

[18] M. Qasim and V. Khadkikar, "Application of artificial neural networks for shunt active power filter control," *IEEE Trans. Ind. Informat.*, vol. 10, no. 3, pp. 1765–1774, Aug. 2014.

[19] S.-G. Jeong and M.-H. Woo, "DSP-based active power filter with predictive current control," *IEEE Trans. Ind. Electron.*, vol. 44, no. 3, pp. 329–336, Jun. 1997.

[20] A. Bhattacharya and C. Chakraborty, "A shunt active power filter with enhanced performance using ANN-based predictive and adaptive controllers," *IEEE Trans. Ind. Electron.*, vol. 58, no. 2, pp. 421–428, Feb. 2011.

[21] M. Odavic, V. Biagini, P. Zanchetta, M. Sumner, and M. Degano, "One-sample-period-ahead predictive current control for high-performance active shunt power filters," *IET Power Electron.*, vol. 4, no. 4, pp. 414–423, Apr. 2011.

[22] S. Bayhan and H. Abu-Rub, "Predictive control of power electronic converters," in *Power Electronics Handbook*, 4th ed., M. H. Rashid, Ed. London, U.K.: Butterworth-Heinemann, 2018, pp. 1325–1338, doi: 10.1016/B978-0-12-811407-0.00044-1.

[23] R. Panigrahi, B. Subudhi, and P. C. Panda, "Model predictive-based shunt active power filter with a new reference current estimation strategy," *IET Power Electron.*, vol. 8, no. 2, pp. 221–233, 2015.

[24] L. Tarisciotti, A. Formentini, A. Gaeta, M. Degano, P. Zanchetta, R. Rabbeni, and M. Pucci, "Model predictive control for shunt active filters with fixed switching frequency," *IEEE Trans. Ind. Appl.*, vol. 53, no. 1, pp. 296–304, Jan./Feb. 2017.

[25] O. Kukrer, H. Komurcugil, R. Guzman, and L. G. de Vicuna, "A new control strategy for three-phase shunt active power filters based on FIR prediction," *IEEE Trans. Ind. Electron.*, vol. 68, no. 9, pp. 7702–7713, Sep. 2021.

[26] V. Muneer and A. Bhattacharya, "Peak power demand management by using SMC-controlled three-level CHB-based three-wire and four-wire SAPF," *IEEE Trans. Ind. Informat.*, vol. 17, no. 8, pp. 5270–5281, Aug. 2021.

[27] P. Acuña, L. Morán, M. Rivera, R. Aguilera, R. Burgos, and V. G. Agelidis, "A single-objective predictive control method for a multivariable single-phase three-level NPC converter-based active power filter," *IEEE Trans. Ind. Electron.*, vol. 62, no. 7, pp. 4598–4607, Jul. 2015.

[28] K. Antoniewicz, M. Jasinski, M. P. Kazmierkowski, and M. Malinowski, "Model predictive control for three-level four-leg flying capacitor converter operating as shunt active power filter," *IEEE Trans. Ind. Electron.*, vol. 63, no. 8, pp. 5255–5262, Aug. 2016.

[29] M. Schweizer and J. W. Kolar, "Design and implementation of a highly efficient three-level T-type converter for low-voltage applications," *IEEE Trans. Power Electron.*, vol. 28, no. 2, pp. 899–907, Feb. 2013.

[30] C. D. Townsend, T. J. Summers, J. Vodden, A. J. Watson, R. E. Betz, and J. C. Clare, "Optimization of switching losses and capacitor voltage ripple using model predictive control of a cascaded H-bridge multilevel StatCom," *IEEE Trans. Power Electron.*, vol. 28, no. 7, pp. 3077–3087, Jul. 2013.

[31] A. H. Budhrani, K. J. Bhayani, and A. R. Pathak, "Design parameters of shunt active filter for harmonics current mitigation," *PDPU J. Energy Manage.*, vol. 2, no. 2, pp. 59–65, 2018.

[32] M. A. A. M. Zainuri, M. A. M. Radzi, A. C. Soh, N. Mariun, and N. A. Rahim, "DC-link capacitor voltage control for single-phase shunt active power filter with step size error cancellation in self-charging algorithm," *IET Power Electron.*, vol. 9, no. 2, pp. 323–335, Feb. 2016.

[33] I. Sefa, S. Ozdemir, H. Komurcugil, and N. Altin, "Comparative study on Lyapunov-function-based control schemes for single-phase grid-connected voltage-source inverter with LCL filter," *IET Renew. Power Gener.*, vol. 11, no. 11, pp. 1473–1482, Sep. 2017.

[34] I. Sefa, S. Ozdemir, H. Komurcugil, and N. Altin, "An enhanced Lyapunov-function based control scheme for three-phase grid-tied VSI with LCL filter," *IEEE Trans. Sustain. Energy*, vol. 10, no. 2, pp. 504–513, Apr. 2019.

[35] A. A. Valdez-Fernandez, G. Escobar, D. U. Campos-Delgado, K. O. Mtepele, and P. R. Martinez-Rodriguez, "A model-based controller for a single-phase n-level CHB multilevel converter," *Int. J. Electr. Power Energy Syst.*, vol. 125, Feb. 2021, Art. no. 106454.

[36] J. O. Pinto, R. Macedo, V. Monteiro, L. Barros, T. Sousa, and J. Afonso, "Single-phase shunt active power filter based on a 5-Level converter topology," *Energies*, vol. 11, no. 4, p. 1019, Apr. 2018.

[37] L. Wu and W. Mingli, "Single-phase cascaded H-bridge multi-level active power filter based on direct current control in AC electric railway application," *IET Power Electron.*, vol. 10, no. 6, pp. 637–645, May 2017.

[38] A. Sahli, F. Krim, A. Laib, and B. Talbi, "Model predictive control for single phase active power filter using modified packed U-cell (MPUC5) converter," *Electr. Power Syst. Res.*, vol. 180, Mar. 2020, Art. no. 106139.

HASAN KOMURCUGIL (Senior Member, IEEE) received the B.Sc., M.Sc., and Ph.D. degrees from Eastern Mediterranean University (EMU), Famagusta, Turkey, in 1989, 1991, and 1998, respectively, all in electrical engineering. From 2004 to 2010, he was the Head of the Department of Computer Engineering, EMU. In 2010, he played an active role in preparing the department's first self-study report for the use of the Accreditation Board for Engineering and Technology. In 2010, he was elected as the Board Member of Higher Education, Planning, Evaluation, Accreditation and Coordination Council (YODAK), Northern Cyprus. From 2010 to 2019, he played active role in evaluating the universities in Northern Cyprus. He is currently a full-time Professor with the Department of Computer Engineering, EMU. He is a coauthor of one book chapter. His research interests include power electronics and innovative control methods for power converters. He is a member of the IEEE Industrial Electronics Society. He was a recipient of the Best Presentation Recognitions at the 41st and 42nd Annual Conferences of the IEEE Industrial Electronics Society, in 2015 and 2016. He is the Chair of the Renewable Energy Systems Subcommittee of Power Electronics Technical Committee of Industrial Electronics Society (IES). He served as a Corresponding Guest Associate Editor for the IEEE Transactions on Energy Conversion and a Guest Editor for the IEEE Transactions on Industrial Informatics. He also serves as an Associate Editor for the IEEE Transactions on Industrial Electronics and the IEEE Transactions on Industrial Informatics.

SERTAC BAYHAN (Senior Member, IEEE) received the M.S. and Ph.D. degrees in electrical engineering from Gazi University, Ankara, Turkey, in 2008 and 2012, respectively, where he completed the undergraduate studies and graduated as a valedictorian.

In 2008, he joined the Electronics and Automation Department, Gazi University, as a Lecturer, where he was promoted to Associate Professor, in 2017. From 2014 to 2018, he worked at Texas A&M University, Qatar, as an Associate Research Scientist. He is currently working with the Qatar Environment and Energy Research Institute (QEERI) as a Senior Scientist. He is a Faculty Member, with the rank of an Associate Professor, with the Sustainable Division, College of Science and Engineering, Hamad Bin Khalifa University. He has acquired $13M in research funding and published more than 150 papers in mostly prestigious IEEE journals and conferences. He is also the coauthor of two books and five book chapters.

Dr. Bayhan was a recipient of many prestigious international awards, such as the Research Fellow Excellence Award in recognition of his research achievements and exceptional contributions to the Texas A&M University, in 2018; the Best Paper Presentation Recognition at the 41st and 42nd Annual Conference of the IEEE Industrial Electronics Society, in 2015 and 2016; the Research Excellence Travel Awards at Texas A&M University, in 2014 and 2015; and the Researcher Support Awards from the Scientific and Technological Research Council of Turkey (TUBITAK). Because of the visibility of his research, he has been recently elected as the Chair of the IES Power Electronics Technical Committee. He currently serves as an Associate Editor for IEEE Transactions on Industrial Electronics, IEEE Journal of Emerging and Selected Topics in Industrial Electronics, IEEE Open Journal of the Industrial Electronics Society, and IEEE Industrial Electronics Technology News, and a Guest Editor for the IEEE Transactions on Industrial Informatics.

NAKI GULER (Member, IEEE) received the B.Sc., M.Sc., and Ph.D. degrees in electrical and electronic engineering from Gazi University, Ankara, Turkey, in 2010, 2012, and 2019, respectively. He joined the Department of Electricity and Energy, Gazi University, in 2012. His current research interests include control and applications of power electronic converters, energy conversion, and energy management of renewable sources. He was a recipient of the Best Paper Awards at the 6th ICRERA and 12th CPE-POWERENG conferences.

FREDE BLAABJERG (Fellow, IEEE) received the Ph.D. degree in electrical engineering from Aalborg University, in 1995. He was with ABB-Scandia, Randers, Denmark, from 1987 to 1988. He became an assistant professor, in 1992; an associate professor, in 1996; and a full professor of power electronics and drives, in 1998. Since 2017, he became a villum investigator. In 2017, he became a Honoris Causa at University Politehnica Timisoara (UPT), Romania. He is also a Honoris Causa at Tallinn Technical University (TTU), Estonia. His current research interests include power electronics and its applications, such as in wind turbines, PV systems, reliability, harmonics, and adjustable speed drives. He has published more than 600 journal articles in the fields of power electronics and its applications. He is the coauthor of four monographs and an editor of ten books in power electronics and its applications. He has received 32 IEEE Prize Paper Awards; the IEEE PELS Distinguished Service Award, in 2009; the EPE-PEMC Council Award, in 2010; the IEEE William E. Newell Power Electronics Award 2014; the Villum Kann Rasmussen Research Award 2014; the Global Energy Prize, in 2019; and the 2020 IEEE Edison Medal. He was nominated, in 2014 to 2019, by Thomson Reuters to be between the most 250 cited researchers in engineering in the world. In 2020, he received the prestigious IEEE Edison Award for his extraordinary contribution to the next generation of reliable power electronics technologies with industry. He has been a Distinguished Lecturer of the IEEE Power Electronics Society, from 2005 to 2007, and the IEEE Industry Applications Society, from 2010 to 2011 as well as 2017 to 2018. From 2019 to 2020, he served as the President for IEEE Power Electronics Society. He is the Vice-President of the Danish Academy of Technical Sciences. He was the Editor-in-Chief of the IEEE Transactions on Power Electronics, from 2006 to 2012.

• • •